RSC Advances

PAPER

View Article Online
View Journal | View Issue

Cite this: *RSC Adv.*, 2026, **16**, 13358

Cyclometalated Ir(III) complexes bridged by μ-OH and μ-3,5-bis(4-methoxyphenyl)-pyrazole ligands

Mausami, †[a] Harshita Trivedi, †[a] Ranjan Patra, [b] Ravi Prakash Behere, [c] Biplab Kuila, [c] Sandeep Kumar Singh Patel, [a] Mrituanjay D. Pandey, [c] Biswajit Maiti [c] and Bani Mahanti *[a]

Recent advances of cyclometalated Ir(III) complexes are due to their varied structural features and rich photophysical properties. Having this in mind, in the present investigation neutral, cyclometalated heterobridged Ir(III) dimers [(ppy)$_2$Ir(μ-OH){μ-(PhOMe)$_2$Pz}Ir(ppy)$_2$] (**1**) and [(tpy)$_2$Ir(μ-OH){μ-(PhOMe)$_2$Pz}Ir(tpy)$_2$] (**2**) (ppyH = 2-phenylpyridine; tpyH = 2-(*p*-tolyl)pyridine; (PhOMe)$_2$PzH = 3,5-bis(4-methoxyphenyl)-pyrazole) are synthesized and characterized by various analytical techniques such as NMR, ESI-MS, UV-Vis, emission and cyclic voltammetric studies. Complex **1**, has been also characterized by single crystal X-ray diffraction analysis. Both complexes are found to be emissive in aerated dichloromethane solution with emission maxima centered at around 550 nm for complex **1** and 546 nm for complex **2**. Furthermore, density functional theory (DFT) and time-dependent density functional theory (TDDFT) calculations have been carried out on both complexes **1** and **2** to provide insights into their photophysical characteristics. The observed photophysical properties align well with the DFT and TDDFT results. Our electrochemical investigations demonstrate the stability of the complexes and also the fact that the bridging ligands play an important role in facilitating metal–metal communication within the dimers. In our important findings, we observe a unique interplay of ligand roles where modifying the ancillary ligand does not alter the photophysical properties of the resultant Ir(III) complexes, but are essential for the structural integrity and stability of the complexes. The pyrazole ligand used in the study, 3,5-bis(4-methoxyphenyl)-pyrazole, facilitates the assembly of robust dimeric structures, and the –OH ligand helps shift the spectral properties towards the red end of the spectrum. This study demonstrates that steric modulation can be used to significantly improve the synthesis and isolation of dinuclear Ir(III) complexes without relying on changes in electronic structure. This study provides a clear contrast to prior electronically driven approaches and establishes steric design as a strategy for the rational construction of dimeric cyclometalated Ir(III) complexes. Our results also underscore the significant impact of the bridging ligand on the electronic structure and spectroscopic properties of the cyclometalated Ir(III) complexes, potentially augmenting our understanding of the structure–property variations of such compounds and paving the way for their potential applications.

Received 1st February 2026
Accepted 4th March 2026

DOI: 10.1039/d6ra00878j

rsc.li/rsc-advances

Introduction

Cyclometalated Ir(III) complexes have been the focus of increasing interest in recent years because of their remarkable photophysical properties, attracting sustained interest from research groups worldwide.[1–8] This class of complexes serve as efficient phosphorescence emitters, featuring a luminescence efficiency four times greater than conventional fluorescence-based emitters (in principle).[9–13] This enhanced performance arises from their ability to harvest both singlet and triplet excitons,[9] theoretically achieving 100% quantum yield (Φ_p).[10–14] The quantum yields vary widely, from less than 1% up to 100%. For example, the complex *fac*-tris(2-phenylpyridine) iridium(III) exhibits a quantum yield of 0.97 in dilute 2-MeTHF at room temperature.[15] Experimental yields are often less than 100% because of non-radiative decay, quenching by oxygen, aggregation, thermal population of non-emissive states *etc.*[16] The remarkable photophysical attributes of these complexes are due to spin–orbit coupling (SOC) induced by the heavy metal center of Ir(III), consequently facilitating an accelerated rate of intersystem crossing (ISC) between singlet and triplet excited states.[17–21]

A wide range of experimental and computational studies have examined cyclometalated Ir(III) complexes and identified

[a]*Department of Chemistry, Mahila Mahavidyalaya, Banaras Hindu University, Varanasi-221005, India. E-mail: bani@bhu.ac.in*

[b]*Amity Institute of Click Chemistry Research and Studies, Amity University, Noida, Uttar Pradesh, India*

[c]*Department of Chemistry, Institute of Science, Banaras Hindu University, Varanasi-221005, India*

† Equal contribution.

important rules for changing emission colour by modifying the ligands.[22–28] Although the use of electron-donating or withdrawing substituents for tuning phosphorescence has been well-established,[29] there is still a significant drive to develop phosphors whose emission properties can be more readily tailored by modifying the electronic properties of both cyclometalating and ancillary ligands.[30–32]

Substituted pyrazole derivatives have played an important role in the assembly of phosphorescent Ir(III) complexes and other transition metals due to their ability to display versatile and adaptable coordination modes.[33–36] Previously, Chandrasekhar *et al.* have reported heterobridged cyclometalated Ir(III) dimers (pyrazolate- and hydroxide-bridged) and investigated their photophysical and electrochemical properties. The complexes were found to be emissive, with the emission maxima being red-shifted compared to mononuclear analogues containing substituted pyrazole ancillary ligands. The hydroxy group as a bridging ligand also helped in effectively mediating the metal–metal communications in these systems.[37] Liao *et al.* reported iridium(III) dimers containing bridging pyrazolate ligands. The complexes were found to be volatile and suitable for the fabrication of OLEDs.[38] Building on these findings, we have introduced methoxy substitution (–OMe) into the ancillary 3,5-diphenyl pyrazole ligand backbone to examine its effect on the geometry and luminescence of the resulting complexes. Methoxy groups are known to function as an electron-withdrawing substituent by inductive effect and as an electron-donating substituent by mesomeric effect.[39,40] Incorporation of methoxy (–OMe) groups into the 3,5-diphenyl pyrazole backbone is expected to introduce substantial steric bulk at the periphery of the complex. Consequently, such steric modulation is anticipated to promote the controlled and selective assembly of well-defined dinuclear species, while enhancing their stability and enabling their efficient isolation. We further anticipated that modulation of the steric bulk of the ligand would afford dimeric N, N-bridged complexes while limiting the formation of monomers and product mixtures, as was observed when 3,5-phenyl methyl pyrazole was employed as an ancillary ligand.[37]

Kamrul Hasan *et al.* have previously reported on tuning the emission towards the red in cationic Ir(III) complexes through methoxy substitution of the cyclometalating ligand.[41] Davies *et al.* have reported tuning of emission wavelength and redox properties by varying substituents, including the methoxy group in 3-substituted 1-phenylpyrazoles, where the pyrazole ligand has been employed as a cyclometalating ligand.[42] However, to the best of our knowledge, an investigation into methoxy group substitution in the ancillary diphenyl pyrazole ligand backbone has not been undertaken until now. Previous studies on dinuclear cyclometalated Ir(III) complexes have mainly focused on electronic tuning by modifying cyclometalating or ancillary ligands to adjust emission color or excited state behavior.[43,44] While this strategy has proven effective for adjusting photophysical properties, it has comparatively little impact on the practical aspects of dinuclear complex formation, particularly with respect to isolation of discrete bimetallic species. In some cases, low yields, or difficulties in purification have hindered systematic exploration of dinuclear species.[4] Bulky substituents on ancillary ligands are known to improve photophysical properties in cyclometalated Ir(III) complexes by affecting steric environments, showing the utility of steric design strategies.[45] We propose that judicious steric modification of ligands at positions remote from the Ir(III) coordination core could provide an independent and underexplored strategy to control the formation of dinuclear cyclometalated Ir(III) complexes.

In this study, we present the synthesis, characterization, and detailed photophysical and electrochemical investigation of cyclometalated Ir(III) dimers featuring two different bridging ligands, $[(ppy)_2Ir(\mu\text{-}OH)\{\mu\text{-}(PhOMe)_2Pz\}Ir(ppy)_2]$ (**1**) and $[(tpy)_2Ir(\mu\text{-}OH)\{\mu\text{-}(PhOMe)_2Pz\}Ir(tpy)_2]$ (**2**), where ppyH = 2-phenylpyridine, tpyH = 2-(*p*-tolyl)pyridine, and $(PhOMe)_2PzH$ = 3,5-bis(4-methoxyphenyl)pyrazole. DFT and TDDFT calculations were carried out to further elucidate the photophysical behaviour of these complexes. One of our key findings in this work is that the introduction of methoxy (–OMe) groups into the 3,5-diphenyl pyrazole backbone leads to an increase in steric bulk at positions far from the metal coordination site. This change strongly affects how the dinuclear complexes form. The added steric hindrance makes the dimeric complexes easier to isolate, and directs the reaction toward the formation of a single, well-defined dimer rather than a mixture of products. Overall, our findings deepen the understanding of structure–property relationships and photophysical behaviour in cyclometalated Ir(III) systems and provide useful guidance for the rational design of iridium based phosphorescent materials.

Results and discussion

Synthesis and characterization

The heteroleptic Ir(III) dimers $[(ppy)_2Ir(\mu\text{-}OH)\{\mu\text{-}(PhOMe)_2Pz\}Ir(ppy)_2]$ (**1**), $[(tpy)_2Ir(\mu\text{-}OH)\{\mu\text{-}(PhOMe)_2Pz\}Ir(tpy)_2]$ (**2**) were isolated as orange solids by following the general two-step synthetic protocol. The first step involves the synthesis of the organometallic, cyclometalated chloro-bridged iridium(III) dimer precursor complexes, which are $[(ppy)_2Ir(\mu\text{-}Cl)]_2$ and $[(tpy)_2Ir(\mu\text{-}Cl)]_2$, respectively. The Nonoyama protocol was followed for the synthesis of the aforementioned precursors.[46] The ancillary ligand $(PhOMe)_2PzH$ = 3,5-bis(4-methoxyphenyl)-pyrazole) was synthesized by condensation of 1,3-bis(4-methoxyphenyl)propane-1,3-dione with hydrazine hydrate in ethanol as solvent.[47] In the second step, the iridium(III) dimers underwent a bridge splitting reaction on reaction with sodium methoxide, followed by 3,5-bis(4-methoxyphenyl)-pyrazole in dichloromethane solvent, affording the desired asymmetrically bridged cyclometalated Ir(III) dimers $[(ppy)_2Ir(\mu\text{-}OH)\{\mu\text{-}(PhOMe)_2Pz\}Ir(ppy)_2]$ (**1**) and $[(tpy)_2Ir(\mu\text{-}OH)\{\mu\text{-}(PhOMe)_2Pz\}Ir(tpy)_2]$ (**2**) with satisfactory yields (Scheme 1).

Single crystals of **1** suitable for X-ray analysis were obtained by slow evaporation in dichloromethane solution, with a few drops of methanol added for layering at room temperature. The ORTEP diagram for the cyclometalated heterobridged Ir(III) dinuclear complex **1**, which crystallized in the triclinic system with space group $P\bar{1}$, is shown in Fig. 1. Crystallographic data are presented in Table 1, while some selected bond lengths and

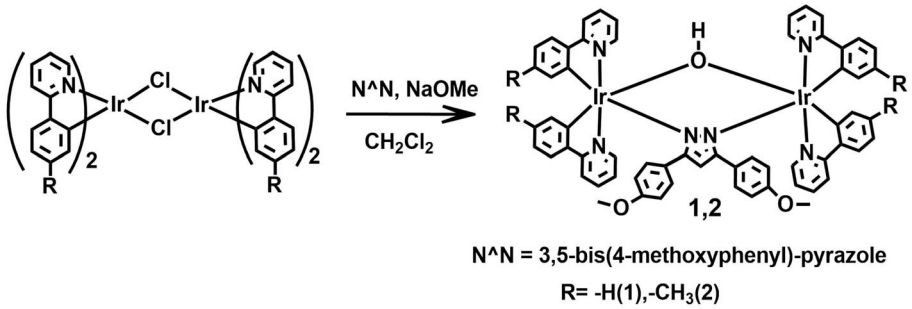

Scheme 1 Synthesis of complexes **1–2**.

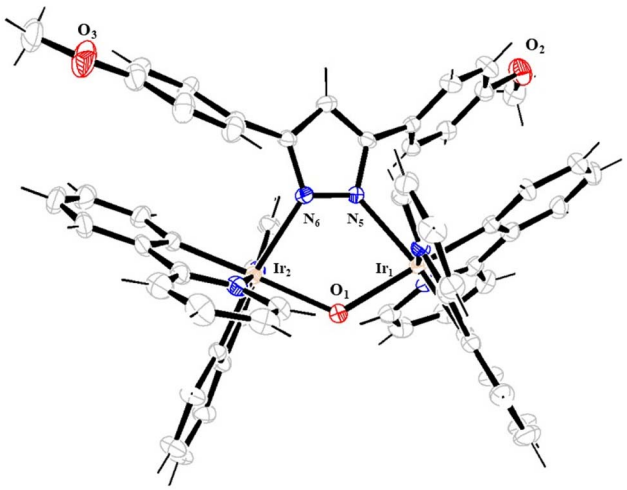

Fig. 1 ORTEP diagram of complex **1** with thermal ellipsoids at the 20% probability limit.

bond angles are listed in Table 2. The geometry around Ir(III) metal atom in each monomeric unit is distorted octahedral, with the cyclometalating ligand arranged in a *trans N,N* and *cis* C–C configuration. The 3,5-bis(4-methoxyphenyl)-pyrazole ancillary ligand coordinates in μ-η^1:η^1 fashion. The coordination of the two iridium centers with the bridging ligands (substituted pyrazolate and hydroxide) leads to the formation of a puckered five-membered [Ir_2N_2O] ring. The puckered conformation of the five-membered ring [Ir_2N_2O] is reflected in the Ir–O–Ir bond angle (124.6°), which is considerably larger than the bond angles O1–Ir1–N5 (81.0°) and O1–Ir2–N6 (81.4°) in the ring. The Ir–N bond lengths of cyclometalating ligand (1.997–2.064 Å) are slightly shorter compared to the Ir–N distance (2.187–2.201 Å) of the bridging pyrazolate ligand, likely due to the strong *trans* influence cyclometalating ligand's C atom. The Ir–C, Ir–O and non-bonding Ir⋯Ir bond lengths are 1.993–2.019 Å, 2.143–2.147 Å and 3.798 Å, respectively, which fall within the typical ranges for similar systems. The *trans* N–Ir–N and Ir–O–Ir

Table 1 Crystallographic data of complex **1**

Empirical formula	$C_{61}H_{47}Ir_2N_6O_3$
Formula weight	1400.93
Temperature/K	293(2)
Crystal system	Triclinic
Space group	$P\bar{1}$
a/Å	11.9421(2)
b/Å	15.4721(2)
c/Å	15.7074(2)
α/°	86.0060(10)
β/°	89.7850(10)
γ/°	70.5140(10)
Volume/Å^3	2728.78(7)
Z	2
$\rho_{calc.}$/g cm^{-3}	1.705
μ/mm^{-1}	10.228
F(000)	1372.0
Crystal size/mm^3	0.28 × 0.26 × 0.2
Radiation	Cu Kα (λ = 1.54184)
2Θ range for data collection/°	5.642–136.2
Index ranges	$-14 \le h \le 14$, $-18 \le k \le 18$, $-14 \le l \le 18$
Reflections collected	17 624
Independent reflections	17 624 [R_{int} = 2.19, R_{sigma} = 0.0205]
Data/restraints/parameters	17 624/1/653
Goodness-of-fit on F^2	1.076
Final R indexes [$I \ge 2\sigma$ (I)]	R_1 = 0.0615, wR_2 = 0.1778
Final R indexes [all data]	R_1 = 0.0660, wR_2 = 0.1840
Largest diff. peak/hole/e Å^{-3}	4.27/−1.25

Table 2 Selected bond lengths (Å) and angles (°) of complex **1**

Bond length	(Å)
Ir(1)–O(1)	2.147(6)
Ir(1)–N(5)	2.201(6)
Ir(1)–C(11)	2.011(9)
Ir(1)–C(12)	1.993(9)
N(2)–Ir(1)–N(1) (*trans* bond length)	2.050(6)⋯2.064(6)
Ir(2)–O(1)	2.143(6)
Ir(2)–N(6)	2.187(6)
Ir(2)–C(33)	2.007(9)
Ir(2)–C(44)	2.019(8)
N(4)–Ir(2)– N(3) (*trans* bond length)	2.038(7)⋯1.997(8)

Bond angle	(°)
N(4)–Ir(2)–N(3) (*trans* bond angle)	171.3(3)
N(2)–Ir(1)–N(1) (*trans* bond angle)	172.3(3)
Ir(1)–O(1)–Ir(2)	124.6(3)
N(6)–Ir(2)–O(1)	81.4(2)
N(5)–Ir(1)–O(1)	81.0(2)
N(3)–Ir(2)–C(33)	80.1(4)
N(4)–Ir(2)–C(44)	79.9(3)
N(2)–Ir(1)–C(12)	80.2(3)
N(1)-Ir(1)-C(11)	79.9(3)

bond angles are approximately 171.3°–172.3° and 124.6°, respectively, and are consistent with values reported in previous studies.[37]

Detailed characterization of both complexes **1** and **2** has been carried out by various analytical techniques such as FT-IR, ^{1}H NMR, ^{13}C NMR, COSY NMR (^{1}H–^{1}H), HSQC NMR (^{1}H–^{13}C) and ESI-MS. The ^{1}H NMR spectrum of both complexes **1** and **2** shows a sharp singlet peak at 6.00 ppm and 5.97 ppm, respectively, corresponding to the pyrazole (–CH_{11}) proton (Fig. S3 and S4, SI). The pyrazole (–CH_{11}) acts as a characteristic peak for the identification of both compounds. Methoxy substituents in both **1** and **2** show a singlet with a chemical shift value of 3.65 ppm (Fig. S3 and S4, SI).

In the COSY NMR (^{1}H–^{1}H) for complex 1 (Fig. S5, SI), two distinct doublets appear at 8.27 ppm and 7.90 ppm in the downfield region of the spectra attached to electronegative nitrogen heteroatoms corresponding to (H_1 and $H_{1'}$) and both the protons cross-couple with (H_2 and $H_{2'}$) at 6.51 ppm and 6.76 ppm. Two doublets appear in the upfield region at 5.60 ppm and 5.80 ppm, corresponding to protons H_5 and $H_{5'}$ showing cross-coupling with (H_6 and $H_{6'}$). Aromatic protons of the phenyl ring H_{10} and H_9 (pyrazole) appear at 6.15 ppm and 6.32 ppm, cross-couple with each other, and split into two intense doublets. The ^{1}H–^{1}H couple NMR spectrum of **2** (Fig. S6, SI) shows two sharp singlets appearing at 1.83 ppm and 1.88 ppm in the aliphatic region corresponding to $CH_{3(7)}$ and $CH_{3(7')}$ protons. In the aromatic region, two sharp singlets appear at 5.62 ppm and 5.45 ppm, and these peaks correspond to phenyl ring proton H_8 and $H_{8'}$ (cyclometalating ligand). Proton (H_1 and $H_{1'}$) cross couple with (H_2 and $H_{2'}$). Proton H_9 and H_{10} cross-couple with each other and show intense doublets at 6.18 ppm and 6.30 ppm.

Broad band in the IR spectra of **1–2** around 3450 cm^{-1} indicated the presence of the μ-OH group.[48] However, adventitious moisture in KBr pellets used for IR spectral measurements can also produce a similar broad O–H stretching band, rendering IR evidence alone inconclusive. Consequently, ^{1}H NMR spectroscopy, specifically D_2O exchange experiments were employed to confirm the presence of a bridging hydroxide. In the ^{1}H NMR spectra, the bridging hydroxide protons appear as distinct sharp singlets in the upfield region at −2.03 ppm for complex **1** and −2.21 ppm for complex **2**.[48a] This upfield shift is likely due to the ring current from the metalated ligand, combined with the use of dry DMSO as the solvent. Upon the addition of 100 μL of D_2O, these resonances disappeared completely (Fig. S11 and S12, SI). This successful deuterium exchange confirms the labile nature of the protons and provides definitive evidence for the bridging hydroxide moiety. The bridging-OH group arises presumably by hydrolysis of the bridging-OMe group originating from NaOMe used in the reaction.

ESI-MS of both the complexes showed molecular ion peaks as well as [M–OH]$^+$peaks (Fig. S13 and S14, SI). To evaluate the solution stability of the complexes, we performed ^{1}H NMR measurements of complex **1** at three different time intervals: immediately after sample preparation (0 h), after 48 hours, and after 72 hours in $CDCl_3$ at room temperature. The spectra displayed sharp and well-resolved resonances throughout, with no signs of peak broadening, chemical shift changes, or the appearance of new signals indicative of decomposition. These observations confirm that the complex remains intact in solution over the monitored period, supporting its stability under these conditions (Fig. S15, SI).

Photophysical properties in the solution state

The absorption and steady state emission spectra of complexes **1** and **2** were recorded at room temperature in aerated 10^{-5} M dichloromethane solution (Fig. 2 and 3, Table 3). The absorption as well as emission spectral profiles for both the complexes look similar. Both the complexes display intense absorption in the ultraviolet range, between 260 and 300 nm (with molar absorptivity exceeding $\varepsilon > 10^4$ M^{-1} cm^{-1}), attributed to π–π* transitions/spin allowed ^{1}LC within the cyclometalating and ancillary ligand. Additionally, low-energy bands with moderate intensity extending into the visible region, approximately in the wavelength range 350–450 nm, arise from spin-allowed charge transfer transitions. Spin–orbit coupling effects due to the Ir(III) metal center give rise to spin-forbidden transitions, which manifest in the range 450–480 nm, albeit with a lower extinction coefficient. These band assignments were validated through TDDFT (Time dependent density funactional theory) calculations conducted on **1** and **2**, utilizing ground state optimized geometry (Tables S2–S5, SI). The absorption spectral profile and intensity of the bands align with previous findings on bridged dinuclear complexes.[49–52]

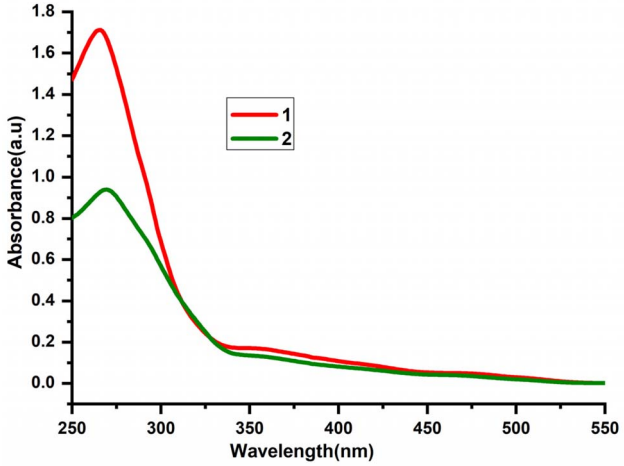

Fig. 2 Absorption spectra of complexes **1** and **2** in dichloromethane solution (10^{-5} M) at room temperature.

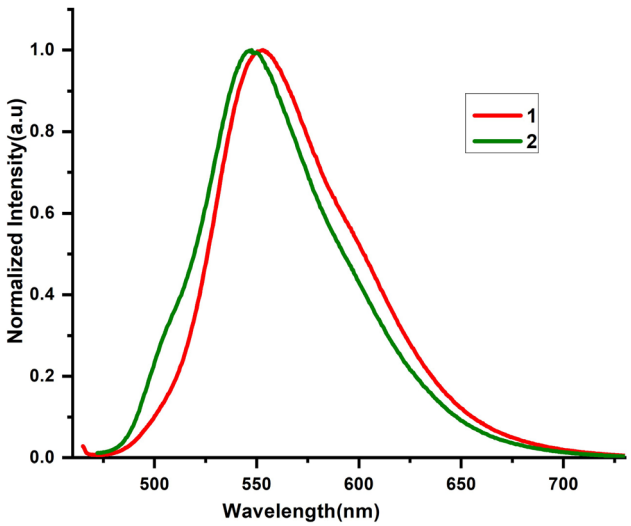

Fig. 3 Emission spectra of complexes **1** and **2** in dichloromethane solution (10^{-5} M) at room temperature (λ_{exc}: 450 nm).

The precursor dimer complex $[Ir(ppy)_2Cl]_2$, (for complex **1**) displays a very weak emission at 520 nm.[53] In comparison, complexes **1** and **2**, which are asymmetrically bridged cyclometalated Ir(III) dimers, $[(ppy)_2Ir(\mu\text{-}OH)\{\mu\text{-}(PhOMe)_2Pz\}Ir(ppy)_2]$ and $[(tpy)_2Ir(\mu\text{-}OH)\{\mu\text{-}(PhOMe)_2Pz\}Ir(tpy)_2]$ respectively, exhibit single, broad, featureless emission bands centered at 550 nm and 546 nm (Fig. 3). This represents a red shift in the emission relative to the precursor complex $[Ir(ppy)_2Cl]_2$. Since the bridging ancillary 3,5-bis(4-methoxyphenyl)-pyrazolate ligand contributes minimally to the HOMO and LUMO, the observed red shift is likely attributable to the bridging OH. The photoluminescence spectra of diiridium complexes bridged by oxamidato ligands reported by Bryce and co-workers display broad, well-defined, and featureless peaks, resembling those observed for complexes **1** and **2**.[54] Zysman-Colman and co-workers reported a series of four formyl-substituted μ-dichloro bridged iridium(III) dimers.[53] Structurally, however, the complexes reported differ from complexes **1** and **2**. Among these, two complexes displayed emission profiles as single, broad, featureless bands similar to those of complexes **1** and **2**, though their emission maxima differed. Such emission features are characteristic of dominant ^{3}MLCT (metal to ligand charge transfer) character with minimal contribution from ligand-centred ^{3}LC (ligand-centred) states. DFT calculations on the aforementioned formyl-substituted μ-dichloro bridged iridium(III) dimers revealed that the HOMO is distributed across the iridium dimer with substantial electron density localized on the iridium centers, the phenyl rings of the cyclometalating ligands, and the μ-Cl bridge. This distribution signifies effective electronic communication between the two iridium atoms mediated by the μ-Cl bridge, analogous to the role of the μ-OH bridge in our complexes. Overall, the emission spectra features correspond well with existing literature observations.[53,55] However, the modification of the pyrazole ligand backbone by introduction of a methoxy substituent (–OMe) does not exert any clear effect on the photophysical properties. The quantum yields of the complexes are 0.06 to 0.05 for **1** and **2**, respectively, which were determined relative to the complex $[Ir(ppy)_2(bpy)]PF_6$ (Φ_{CH_3CN} = 0.0622) in optically dilute solutions.[56] The chloro-bridged Ir(III) precursor complexes are known to be poorly emissive; thus in the current instance, complexes **1** and **2** are better emitters compared to their parent complex. The quantum yields observed for **1** and **2** are also comparable with previous findings in the literature.[57–59] Diiridium cyclometalated Ir(III) complexes are generally characterized by low photoluminescent quantum yields. Although the complexes presented in this work show enhanced quantum yields compared to some literature examples, their values remain in the low range and are still lower than those observed for mononuclear Ir(III) complexes.

It must be emphasized at this point that even though the photophysical properties of the resultant complexes could not be tuned by modification of the ancillary ligand structure, the overall importance of the ancillary ligand cannot be undermined. In our particular case, the steric effect of the ancillary

Table 3 Photophysical properties of **1–2** at 25 °C

Complex	Absorption[a] λ_{max} (nm); 10^{-4} ε (M^{-1} cm^{-1})	Emission[a] λ_{max} (nm)	Solid-state emission[b] λ_{max} (nm)	Φ^c
1	265(17.1), 352(1.74), 418(0.89), 473(0.46)	550	564	0.06
2	269(9.41), 354(1.32), 414(0.70), 463(0.40)	546	564	0.05

[a] Spectral data for both the complexes were recorded in 10^{-5} M dichloromethane solution at room temperature, for emission (λ_{exc} = 450 nm). [b] Solid state emission recorded at λ_{exc} = 450 nm. [c] Quantum yields were determined using $[Ir(ppy)_2(bpy)]PF_6$ (Φ_{CH_3CN} = 0.0622) as reference in aerated solution.

3,5-bis(4-methoxyphenyl)-pyrazole ligand plays an important role in the overall assembly of the dimeric cyclometalated Ir(III) complexes. Earlier studies have shown that, using the same experimental conditions as those employed for the synthesis of complexes **1** and **2**, the reaction of $[(ppy)_2Ir(\mu\text{-}Cl)]_2$ with 3(5)-methyl-5(3)-phenyl pyrazole (PhMePzH) yields a cyclometalated heterobridged Ir(III) dimer, $[(ppy)_2Ir(\mu\text{-}OH)(\mu\text{-}PhMePz)Ir(ppy)_2]$, along with a heteroleptic monomer, $[(ppy)_2Ir(PhMePz)Cl]$.[37] This outcome suggests that reducing the steric bulk of the ancillary ligand leads to the formation of a product mixture. The emission spectrum of the aforementioned heterobridged dimer, which contains a bridging –OH group, exhibits a single emission band at 550 nm similar to that observed for complexes **1** and **2**. In contrast, the heteroleptic mononuclear complex, which lacks the bridging –OH, shows vibronically structured emission bands with an emission maximum at 497 nm. This highlights the influence of the bridging –OH ligand, as evidenced by the redshift in the emission spectrum.

Theoretical calculations

DFT and TDDFT calculations on complex **1** and **2** were conducted to probe their observed photophysical properties and also to understand the impact of methoxy substitution on the ancillary pyrazole ligand backbone.

The key optimized geometry parameters for **1** and **2** in the ground state (S0) at the PBE0 level, together with the experimental value for **1** is shown in Table S1 (SI). The optimized structure obtained by DFT calculations of complex **1** is shown in Fig. 4, which shows that the complex exhibits a distorted octahedral geometry. For complex **1**, the calculated Ir–C bond lengths are 2.000 and 1.999 Å, which align closely with the experimental values of 2.011 and 2.007 Å, respectively. The calculated Ir–N *trans* bond lengths are 2.032, 2.021, 2.032, and 2.020 Å, while the corresponding experimental values are 2.050, 2.064, 2.038, and 1.997 Å. For the bridging pyrazolate ligands, the calculated Ir–N distances are 2.170 and 2.172 Å, while the experimental values are 2.187 and 2.201 Å. The Ir–O and non-bonding Ir···Ir distances are calculated as 2.118–2.119 Å and 3.782 Å, respectively, whereas the experimental measurements are 2.147–2.143 Å and 3.798 Å. The calculated bond angles also show good agreement with experimental data. For complex **2**, no experimental structural data are available. However, its calculated structural parameters show a strong correlation with the experimental values observed for complex **1**, suggesting an identical structural arrangement. In complex **2**, the calculated Ir–C bond lengths are 2.000 and 2.001 Å, while the Ir–N bond lengths in the *trans* positions are 2.033, 2.022, 2.022, and 2.034 Å. For the bridging pyrazolate ligands, the Ir–N distances are calculated to be 2.165 and 2.177 Å. The Ir–O bond length and the non-bonding Ir···Ir separation are determined to be 2.117 Å and 3.781 Å, respectively. The *trans* N–Ir–N and Ir–O–Ir bond angles are approximately 172.0° and 126.5°, respectively. All other calculated bond angles also closely match the experimental values of **1**, supporting the conclusion that both iridium centers adopt a distorted octahedral geometry. DFT optimized structure of **2** is given in Fig. S17.

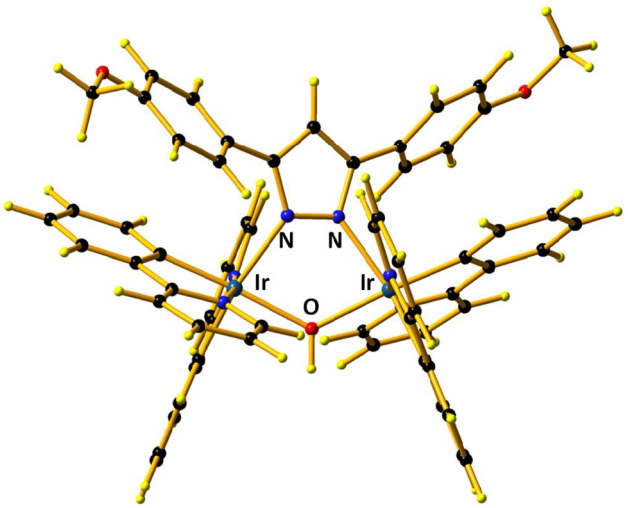

Fig. 4 Optimized geometry parameters of complex **1** in the ground state (S_0) at the PBE0/LANL2TZ/D95V level.

The frontier molecular orbital compositions of complex **1** are given in Table 4. Some selected molecular orbitals with the contour plots are depicted in Fig. 5. The computational results indicate that HOMO, HOMO−1 and HOMO−2 predominantly reside on the cyclometalated ligand (2-phenylpyridine) and the iridium atom, whereas the LUMO, LUMO+1 and LUMO+2 orbitals are primarily concentrated on the cyclometalated ligand. This orbital distribution aligns well with the anticipated characteristics of these complexes and also with literature reports.[60,61] The bridging ancillary 3,5-bis(4-methoxyphenyl)-pyrazolate ligand contributes minimally to both the HOMO and LUMO. However, the HOMO−2 orbital is significantly concentrated on the bridging hydroxide ligand (16.1%). Thus, the use of a methoxy substituent on the pyrazole ligand backbone has minimal effect on the tuning of the HOMO–LUMO gap. The computational results of **2** are given in SI (Fig. S17 and S18). Frontier molecular orbitals of **2** resemble those of **1**. This indicates that varying the substituents on the cyclometalated ligand (C^N), such as adding a methyl group in the phenyl ring of the C^N ligand, does not have any significant effect on the spectral properties.

TDDFT calculations were also performed for both **1** and **2** by utilizing the polarizable continuum model (PCM) with dichloromethane as the solvent. The results show good correlation with experimentally obtained data, albeit with some

Table 4 Molecular orbital composition (%) in the ground state at the PBE0/LANL2TZ/D95V level for complex **1**

Orbital	Energy (eV)	Main bond nature
LUMO+3	−1.137	L_C (92.0%)
LUMO+2	−1.207	L_C (92.3%)
LUMO+1	−1.306	L_C (93.7%)
LUMO	−1.491	L_C (93.8%)
HOMO	−4.930	Ir-d (35.3%) + L_C (51.9%)
HOMO−1	−5.052	Ir-d (38.9%) + L_C (45%)
HOMO−2	−5.091	Ir-d (38.3%) + L_C (38.1%) + L_{OH} (16.1%)
HOMO−3	−5.478	Ir-d (37.3%) + L_C (27.7%) + L_A (32.8%)

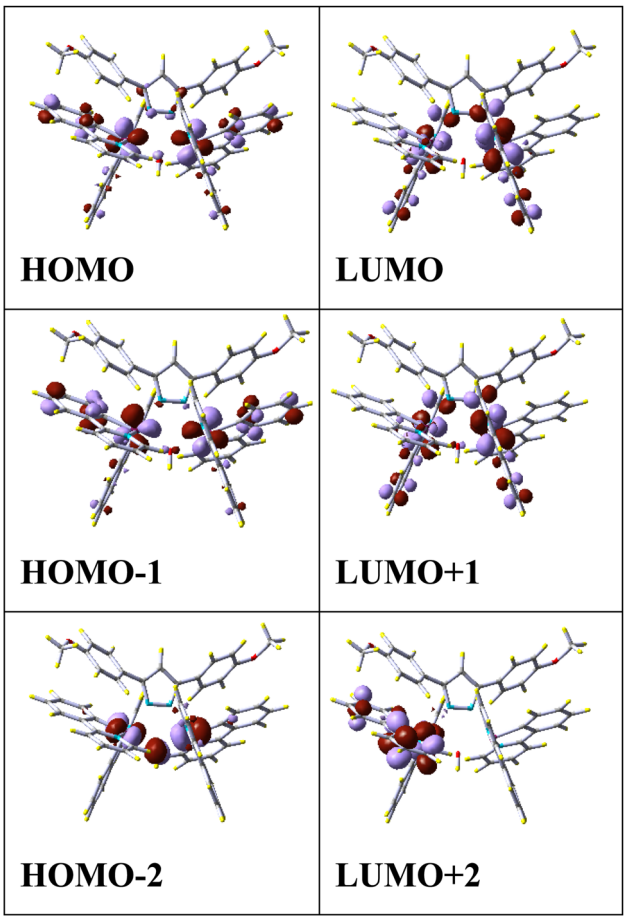

Fig. 5 Relevant molecular orbitals of complex **1** (iso value = 0.04) obtained from DFT calculations at the PBE0/LANL2TZ/D95V level.

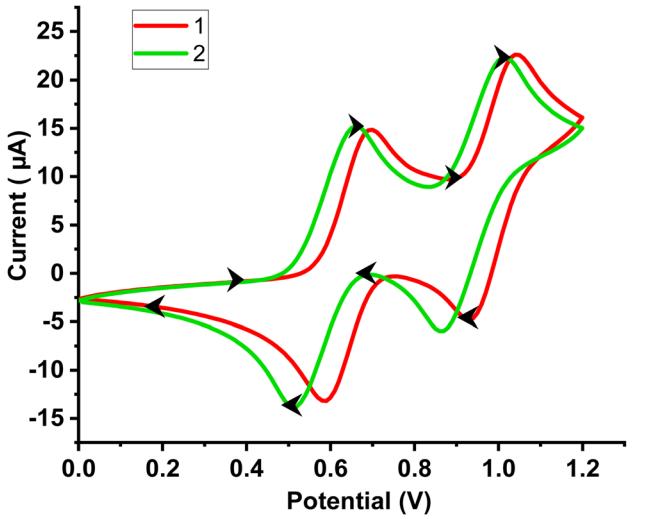

Fig. 6 Cyclic voltammogram of complexes **1**, **2** recorded at room temperature in dichloromethane (1 mM) containing 0.1 M $TBAPF_6$ electrolyte, with a scan rate of 100 mV s^{-1}, starting from 0.0 V.

Table 5 Half-wave redox potentials (*vs.* $Ag/AgNO_3$) of **1–2** at 25 °C

Complex	$E_1^{1/2,ox}/V^a$ ($\Delta E_p/mV$)^b	$E_2^{1/2,ox}/V^a$ ($\Delta E_p/mV$)^b
1	0.64 (115)	0.99 (120)
2	0.58 (156)	0.93(150)
E^o (Fc^+/Fc)^c	0.50 (120)	

^{a} Recorded in dichloromethane solution containing 0.001 M iridium complexes, $E_{1/2} = 1/2(E_{pa} + E_{pc})$, where E_{pa} and E_{pc} are anodic and cathodic peak potentials, respectively. ^{b} $\Delta E_p = E_{pa} - E_{pc}$. ^{c} The Fc^+/Fc redox couple is used as an internal standard reference.

deviations (Tables S2–S5, SI). The lowest energy singlet absorption is dominated by Ir(d) + $L_C \rightarrow L_C$ transitions, which can be assigned to mixed ML_CCT, IL_CCT character. The lowest singlet–triplet excitation energies exhibit ML_CCT, IL_CCT, and $L_{OH}L_CCT$ nature. Importantly, the bridging 3,5-bis(4-methoxyphenyl)-pyrazolate ligand has little involvement in the lowest-energy excited states, indicating that substituent changes on this ligand are unlikely to substantially alter the spectroscopic characteristics of the complexes.

Electrochemical studies

Electrochemical properties of complexes **1–2** were studied by cyclic voltammetry (CV), which was conducted in dry dichloromethane solvent (Fig. 6, Table 5). The complexes display two consecutive one-electron steps (redox couple) corresponding to $Ir^{IV}Ir^{III}/Ir^{III}Ir^{III}$ and $Ir^{IV}Ir^{IV}/Ir^{IV}Ir^{III}$. Complexes **1** and **2** differ in the substitution pattern of the cyclometalating phenylpyridine ligands. This difference affects their oxidation potentials: methyl-substituted complex **2** $[(tpy)_2Ir(\mu\text{-}OH)\{\mu\text{-}(PhOMe)_2Pz\}Ir(tpy)_2]$ is oxidized at a more negative potential (0.58 V, couple 1 and 0.93 V, couple 2) compared to unsubstituted complex **1** $[(ppy)_2Ir(\mu\text{-}OH)\{\mu\text{-}(PhOMe)_2Pz\}Ir(ppy)_2]$ (0.64 V, couple 1 and 0.99 V, couple 2) *versus* Ag^+/Ag, respectively. For the previously reported heterobridged complexes lacking methoxy substituents, oxidation peaks were observed at 0.62 V (couple 1) and 0.95 V (couple 2).[37] The corresponding methoxy-substituted complex (Complex **1**) exhibits nearly identical redox potentials, indicating that the introduction of the methoxy group exerts only a minor electronic effect. Although methoxy substituents are typically electron-donating through mesomeric effect and are expected to shift the reduction potential negatively, in this system, the methoxy groups are pendant and not directly attached to the pyrazole ring. As a result, their electron-donating contribution is minimal. Complex **1** exhibit reversible electrochemical behaviour, while complex **2** displays quasi-reversible behaviour. Within the accessible potential range of the solvent, no reduction processes occurred.

Rocha and co-workers reported a mixed μ-pyrazolate and μ-alkoxide bridged dimer of $Ru(bpy)_2$ moiety.[50] The cyclic voltammogram of the complex in acetonitrile exhibited two one-electron oxidation processes at 0.09 and 0.71 V *versus* Ag^+/Ag, with a large peak separation (ΔE_p) of 620 mV. Large comproportionation constant (K_c) value of 3.0×10^{10} indicated strong electronic communication between the two redox centers.[50] Chandrasekhar *et al.* reported heterobridged cyclometalated Ir(III) dimers featuring substituted pyrazolate and hydroxy

bridges.[37] These complexes displayed two sequential one-electron oxidation steps with moderate peak separations of 332, 338, and 368 mV. Comparable behaviour is observed for our heterobridged iridium(III) complexes. The separation between redox couples ($\Delta E_{1/2}$) for complex **1** is 340 mV and for complex **2** is 350 mV, which gives a comproportionation constant (K_c) of 5.6×10^5 and 8.3×10^5, respectively. This indicates a stabilized mixed valence state of $Ir^{IV}Ir^{III}$, which, according to Robin-Day classification, belongs to class II, characterised by moderate electronic coupling.[49,62] This also indicates communication between the two iridium centers, which may be aided by the presence of a bridging hydroxide ligand. In contrast, the parent dimer $[Ir(ppy)_2Cl]$ exhibits two one-electron oxidation waves with a smaller peak separation of 260 mV, indicating weaker metal–metal interaction mediated by the μ-Cl bridges.[53]

Conclusions

In this study, we have presented heterobridged cyclometalated Ir(III) dimers featuring substituted pyrazole and hydroxide bridges. Introduction of a methoxy substituent in the ancillary pyrazole ligand backbone affords dimeric complexes as anticipated; however, the methoxy substituent does not exert any significant effect on the photophysical properties.

The emission spectra of the heterobridged dimers **1** and **2**, which feature a bridging –OH group, display characteristics similar to those of previously reported heterobridged analogues such as $[(ppy)_2Ir(\mu\text{-}OH)(\mu\text{-}PhMePz)Ir(ppy)_2]$ and $[(tpy)_2Ir(\mu\text{-}OH)(\mu\text{-}Ph_2Pz)Ir(tpy)_2]$. These dimeric complexes show a single emission peak centered around 550 nm. In contrast, reported heteroleptic mononuclear complexes like $[(ppy)_2Ir(PhMePz)Cl]$ and $[(ppy)_2Ir(PhMePz)OH]$, which contain terminal chloride and hydroxide groups, exhibit vibronically structured emission bands with maxima at 497 nm and 513 nm, respectively. This indicates that incorporating a hydroxide bridge leads to a bathochromic shift in the emission bands.

Theoretical DFT and TDDFT calculations provided additional insights into the photophysical properties of these compounds, confirming that only the μ-OH bridge influences the HOMO levels in the diiridium complexes.

Electrochemical investigations further highlight that only the μ-OH bridge plays an important role in facilitating metal–metal communication within the diiridium complexes. Although the ancillary pyrazole ligand does not significantly affect the photophysical properties, it remains an important component of the complexes. These ligands are essential for the stability and formation of the overall structure of the complexes. Since the methoxy groups are located at the para positions of the peripheral phenyl rings rather than directly on the pyrazolate scaffold, their electronic impact on the complex is expected to be minimal. These substituents were mainly introduced at this position to facilitate the formation of dimeric complexes, as the less bulky groups tends to yield monomeric complexes and product mixtures. The added steric hindrance improves the ease of isolation of diiridium species, and directs the reaction towards the formation of a single, well defined dimer instead of a mixture of products. Incorporating substituents with greater ability to influence electronic properties such as C_6H_4-4-NO_2 ($\sigma = 0.25$), could result in more significant changes in the photophysical properties. Exploring such electronically tuned systems is a promising direction, and we intend to pursue this in future studies.

Overall, our findings underscore the significant impact of the bridging ligand on the electronic structure and spectroscopic properties of these Ir(III) dimers, offering new perspectives for the basic understanding of structure and photophysical properties of this emerging class of compounds and might steer further direction for their potential applications in various fields.

Experimental section

General

2-Phenylpyridine was purchased from Sigma Aldrich, while 2-(*p*-tolyl)pyridine, 3,5-bis(4-methoxyphenyl)-pyrazole, hydrazine hydrate, and iridium trichloride hydrate were obtained commercially from TCI and were used as such without further purification. Solvents were purified using standard methods and freshly distilled under an inert atmosphere before use, following established procedures. Freshly prepared sodium methoxide was used in the reactions.

Instrumentation

For complex **1**, ^{1}H NMR was recorded at 600 MHz (Bruker Avance neo). ^{13}C spectra for both **1** and **2** were obtained at 150 MHz. Tetramethylsilane $[Si(CH_3)_4]$ was used as the reference. ESI-HR mass analyses were performed on a Waters Micromass Quattro Micro triple quadrupole mass spectrometer in solutions of compounds **1** and **2** in acetonitrile with 20% formic acid. IR spectra (range 4000–400 cm^{-1}) were recorded on a Bruker FT-IR spectrometer as KBr pellets. UV-visible spectra were recorded at room temperature in a Shimadzu UV-1900i UV-vis spectrophotometer in a Shimadzu Eco Cell 10 mm quartz cuvette. C, H and N analyses were carried out in a Euro EA 3000 CHNS-O analyzer. A Cary Eclipse spectrophotometer was used for the measurement of steady-state emission spectra. Quantum yields were determined using $[Ir(ppy)_2(bpy)]PF_6$ ($\Phi_{CH_3CN} = 0.0622$) as the reference compound. Solvents used were all of spectroscopic grade. Cyclic voltammetry studies were performed at room temperature in Palmsens 4 electrochemical workstation using a standard three-electrode electrochemical cell. Platinum electrode (size 3 mm) was used as a working electrode, $Ag/AgNO_3$ as reference electrode (3 M KNO_3), and a platinum-wire as counter electrode. The studies were carried out using 0.1 M $[n\text{-}Bu_4N][PF_6]$ in dichloromethane solutions (dry) of the complexes (1 mM) under nitrogen atmosphere.[63] Ferrocene (Fc^+/Fc) was used as an internal standard ($E^\circ = 0.50$ V in dichloromethane).

Computational details

Complex **1** was modelled using Gaussian 03.[64] Geometry optimization in the ground state was performed in the gas phase

considering the singlet ground state (S_0) by the PBE0 density functional theory (DFT) method.[65,66] Further, vibrational frequency calculation was carried out at the optimized geometry so as to confirm potential energy minima. Frequency calculations showed the absence of imaginary frequencies. The pseudopotential of LANL2TZ basis set and a triple zeta quality basis set LANL2TZ was taken for iridium atoms,[67] D95V basis set was used on all the non-metal atoms.[68] Gauss view was used for the visualization of orbital surfaces. Vmodes was used to determine the percentage contributions of the iridium center and ligands (cyclometalating, ancillary, and –OH) to the respective orbitals.[69] TDDFT calculations were performed with the optimized geometry at the PBE0/LANL2DZ/D95V level of theory by means of the PCM (Polarizable Continuum Model) solvation model in dichloromethane solution.[70] Similar calculations were performed for complex **2** as well.

X-ray crystallography

X-ray diffraction data were collected at 293 K on an XtaLAB Synergy Dualflex diffractometer equipped with a HyPix3000 detector, using Cu Kα radiation (λ = 1.54184 Å). The crystal structure was solved by direct methods using Olex 2 (v2.0).[71] Full-matrix least-squares refinement on F^2 was performed, with all non-hydrogen atoms refined anisotropically. Hydrogen atoms bonded to carbon were placed in geometrically calculated positions and refined using a riding model with default parameters in SHELXL.[72] The structure was solved and refined as a two component twin, with 12 380 and 4156 reflections respectively. The remaining residual electron density corresponds to Fourier ripples, with two residual peaks located at equal distances from each iridium centers. The hydrogen atom bonded to the bridging oxygen could not be located in the Fourier difference map, most likely due to the dominance of the heavy iridium atoms, which limits the detection of light atoms. Attempts to include this hydrogen atom using restraints (DFIX, DANG) did not result in a stable refinement and were therefore omitted. The presence of a bridging –OH group is, however, supported by ^{1}H NMR studies. Disordered solvent molecules could not be modelled directly. Therefore 'mask' was used for modelling. The suggested cavity and number of electrons indicated the presence of one dichloromethane and two methanol molecules. The crystallographic data for complex **1** have been submitted to the Cambridge Crystallographic Data Centre *via* CCDC number 2415220.

Synthesis

Synthesis of [(ppy)$_2$Ir(μ-OH){μ-(PhOMe)$_2$Pz}Ir(ppy)$_2$] (1)

Procedure. The diiridium complex [(ppy)$_2$Ir(μ-Cl)]$_2$ (0.10 g, 0.093 mmol) was dissolved in 30 mL of dichloromethane, followed by the addition of sodium methoxide (0.025 g, 0.47 mmol). The reaction mixture was stirred under a nitrogen atmosphere at room temperature for 2 hours, during which the color of the reaction mixture changed from yellow to orange. Subsequently, the ancillary ligand 3,5-bis(4-methoxyphenyl) pyrazole (0.031 g, 0.11 mmol) was added, and the mixture was stirred for further 12 hours at room temperature. After completion, the solvent was removed under reduced pressure, yielding an oily residue. The addition of diethyl ether induced precipitation of a yellow solid, which was collected by filtration, washed with methanol, and dried. The yield was found to be 0.082 g, 68%.

Characterization data. ^{1}H NMR (600 MHz, DMSO-d_6): δ 8.21 (d, J = 8.1 Hz, 2H), 7.99 (d, J = 5.3 Hz, 2H), 7.88 (t, J = 7.6 Hz, 2H), 7.81 (d, J = 8.1 Hz, 2H), 7.73 (t, J = 7.5 Hz, 2H), 7.68 (d, J = 7.6 Hz, 2H), 7.05–6.97 (m, 4H), 6.69 (dd, J = 14.2, 6.5 Hz, 4H), 6.63 (t, J = 6.2 Hz, 2H), 6.43 (t, J = 7.3 Hz, 2H), 6.26 (t, J = 7.2 Hz, 2H), 6.18 (t, J = 8.1 Hz, 6H), 6.11 (d, J = 8.5 Hz, 4H), 6.00 (s, 1H), 5.71 (d, J = 7.6 Hz, 2H), 5.51 (d, J = 7.6 Hz, 2H), 3.65 (s, 6H), −2.03 (s, 1H). ^{13}C NMR (150 MHz, DMSO) δ: 169.36, 168.44, 159.54, 157.71, 152.72, 152.30, 152.05, 146.84, 145.54, 144.76, 137.73, 136.29, 131.24, 130.62, 128.93, 128.39, 127.84, 124.39, 124.30, 122.68, 120.99, 120.49, 119.33, 119.04, 118.30, 113.04, 55.25. ESI-HRMS: m/z 1298.3318, [M]$^+$; m/z 1281.3353, [M–OH]$^+$. IR (KBr, cm^{-1}) 3435(br), 3051(w), 2918(m), 2843(w), 1652(w), 1602(s), 1535(s), 1494(vs), 1427(s), 1393(s), 1301(w), 1218(m), 1177(s), 1102(w), 1027(s), 835(w), 760(m), 627(w). CHN analysis: mol. formula: $C_{61}H_{48}Ir_2N_6O_3$; calculated: C, 56.47; H, 3.73; N, 6.48. Found: C, 56.83; H, 4.18; N, 6.92.

Synthesis of [(tpy)$_2$Ir(μ-OH){μ-(PhOMe)$_2$Pz}Ir(tpy)$_2$] (2). The synthetic procedure followed was analogous to that of complex **1** with 2-(*p*-tolyl) pyridine as the cyclometalating ligand instead of 2-phenyl pyridine. Quantities involved were as follows:

[(tpy)$_2$ Ir(μ-Cl)]$_2$. (0.100 g, 0.088 mmol), sodium methoxide (0.023 g, 0.44 mmol), 3,5-bis(4-methoxyphenyl)-pyrazole (0.029 g 0.10 mmol). The yield was found to be 0.079 g, 67%.

^{1}H NMR (600 MHz, DMSO-d_6). δ 8.12 (d, J = 8.1 Hz, 2H), 7.92 (d, J = 5.2 Hz, 2H), 7.82 (t, J = 7.6 Hz, 2H), 7.71 (t, J = 9.8 Hz, 2H), 7.67 (t, J = 7.5 Hz, 2H), 7.55 (d, J = 7.8 Hz, 2H), 6.95 (t, J = 6.3 Hz, 2H), 6.90 (d, J = 7.8 Hz, 2H), 6.65 (d, J = 5.3 Hz, 2H), 6.56 (t, J = 6.1 Hz, 2H), 6.50 (d, J = 7.6 Hz, 2H), 6.16 (t, J = 14.9 Hz, 4H), 6.10 (d, J = 8.2 Hz, 4H), 6.06 (d, J = 7.7 Hz, 2H), 5.97 (s, 1H), 5.52 (s, 2H), 5.29 (s, 2H), 3.65 (s, 6H), 1.78 (s, 6H), 1.75 (s, 6H), −2.21 (s, 1H). ^{13}C NMR (150 MHz, $CDCl_3$) δ: 170.19, 169.60, 159.86, 157.91, 153.26, 152.76, 147.91, 142.56, 142.10, 139.25, 137.87, 136.32, 135.05, 133.06, 132.30, 129.60, 129.44, 124.36, 123.73, 122.26, 121.60, 120.17, 119.45, 118.23, 117.68, 113.08, 111.73, 55.66, 22.18, 22.08. ESI-HRMS: m/z 1354.3696, [M]$^+$; m/z 1337.3612, [M–OH]$^+$. IR (KBr, cm^{-1}) 3435(br), 3018(w), 2918(w), 2842(w), 1744(w), 1602(m), 1527(s), 1485(vs), 1427(s), 1310(w), 1218(m), 1168(m), 1027(w), 1127(w), 1018(m), 835(w), 767(m), 618(w). CHN analysis: mol. formula: $C_{65}H_{56}Ir_2N_6O_3$; calculated: C, 57.68; H, 4.17; N, 6.21; found: C, 57.94; H, 4.72; N, 6.85.

Conflicts of interest

The authors declare no conflict of interest.

Data availability

CCDC 2415220 contains the supplementary crystallographic data for this paper.[73]

The data supporting this article have been included as part of the supplementary information (SI). Supplementary information: IR spectra, NMR spectra, ESI-MS spectra, solid-state emission spectra, cyclic voltammetry plot and computational results. See DOI: https://doi.org/10.1039/d6ra00878j.

Acknowledgements

The authors thank funding from Science and Engineering Research Board, India, New Delhi (FILE No. CRG/2021/000980-G) and IoE (Banaras Hindu University, Scheme No. 6031/2020-21) for generously funding the research. We thank Prof. Subrato Bhattacharya and Dr Divya Kushwaha for valuable discussions.

References

1 K. A. King, P. J. Spellane and R. J. Watts, *J. Am. Chem. Soc.*, 1985, **107**, 1431–1432.
2 D. L. Ma, S. Lin, W. Wang, C. Yang and C. H. Leung, *Chem. Sci.*, 2017, **8**, 878–889.
3 M. K. Nazeeruddin, R. Humphry-Baker, D. Berner, S. Rivier, L. Zuppiroli and M. Graetzel, *J. Am. Chem. Soc.*, 2003, **125**, 8790–8797.
4 M. Z. Shafikov, A. V. Zaytsev and V. N. Kozhevnikov, *Inorg. Chem.*, 2024, **63**, 1317–1327.
5 L. E. Cells, K. Nazeeruddin, R. T. Wegh, Z. Zhou, C. Klein, Q. Wang, F. De Angelis, S. Fantacci and M. Grätzel, *Inorg. Chem.*, 2006, **45**, 9245–9250.
6 Y. You, S. Cho and W. Nam, *Inorg. Chem.*, 2014, **53**, 1804–1815.
7 Y. You, S. Lee, T. Kim, K. Ohkubo, W. S. Chae, S. Fukuzumi, G. J. Jhon, W. Nam and S. J. Lippard, *J. Am. Chem. Soc.*, 2011, **133**, 18328–18342.
8 Q. Zhao, M. Yu, L. Shi, S. Liu, C. Li, M. Shi, Z. Zhou, C. Huang and F. Li, *Organometallics*, 2010, **29**, 1085–1091.
9 S. Lee and W. Han, *Inorg. Chem. Front.*, 2020, **7**, 2396–2422.
10 C. Wu, K. Shi, S. Li, J. Yan, Z.-Q. Feng, K.-N. Tong, S.-W. Zhang, Y. Zhang, D. Zhang, L.-S. Liao, Y. Chi, G. Wei and F. Kang, *Energy Chem.*, 2024, **6**, 100120.
11 (*a*) Q. Yang, X. Yang, Y. Wang, Y. Fei, F. Li, H. Zheng, K. Li, Y. Han, T. Hattori, P. Zhu, S. Zhao, L. Fang, X. Hou, Z. Liu, B. Yang and B. Zou, *Nat. Commun.*, 2024, **15**, 7778; (*b*) Z. K. Qin, Y. K. Zhang, H. Tian, Z. C. Pan, M. Q. Wang, L. Cui, J. Y. Wang, L. X. Bao, Y. H. Wang, W. Y. Zhang and M. X. Song, *RSC Adv.*, 2024, **14**, 36895–36901.
12 M. A. Baldo, M. E. Thompson and S. R. Forrest, *Pure Appl. Chem.*, 1999, **71**, 2095–2106.
13 S. Lamansky, P. Djurovich, D. Murphy, F. Abdel-Razzaq, R. Kwong, I. Tsyba, M. Bortz, B. Mui, R. Bau and M. E. Thompson, *Inorg. Chem.*, 2001, **40**, 1704–1711.
14 I. Soriano-Díaz, I. D. Dergachev, S. A. Varganov, E. Ortí and A. Giussani, *J. Phys. Chem. Lett.*, 2025, **16**, 9004–9010.
15 T. Sajoto, P. I. Djurovich, A. B. Tamayo, J. Oxgaard, W. A. Goddard III and M. E. Thompson, *J. Am. Chem. Soc.*, 2009, **131**, 9813–9822.
16 A. Omist, I. D. Dergachev, S. A. Varganov, E. Ort and A. Giussani, *Inorg. Chem.*, 2025, **64**, 8313–8321.
17 I. Soriano-Díaz, I. D. Dergachev, S. A. Varganov, E. Ortí and A. Giussani, *J. Phys. Chem. Lett.*, 2025, **16**, 9004–9010.
18 J. M. Younker and K. D. Dobbs, *J. Phys. Chem. C*, 2013, **117**, 25714–25723.
19 M. Spiegel, *Int. J. Mol. Sci.*, 2025, **26**, 5062.
20 K. S. Bejoymohandas, A. Baschieri, F. Reginato, S. Toffanin, M. Prosa, E. Bandini, A. Mazzanti and F. Monti, *Adv. Opt. Mater.*, 2024, **12**, 2401586.
21 E. Baranoff, S. Fantacci, F. De Angelis, X. Zhang, R. Scopelliti, M. Grätzel and M. K. Nazeeruddin, *Inorg. Chem.*, 2011, **50**, 451–462.
22 N. Singh, G. H. Noh, H. Mubarok, C. W. Kim, M. H. Lee and J. Lee, *Polyhedron*, 2022, **227**, 116096.
23 A. Baschieri, L. Sambri, A. Mazzanti, A. Carlone, F. Monti and N. Armaroli, *Inorg. Chem.*, 2020, **59**, 16238–16250.
24 E. M. Vollbert, C. Ciambrone, W. Lafargue-dit-hauret, C. Latouche, F. Loiseau and P. H. Lanoe, *Inorg. Chem.*, 2022, **61**, 3033–3049.
25 E. A. Katlenok, A. V Rozhkov, R. R. Ramazanov, R. R. Valiev, O. V Levin, D. O. Goryachiy, I. V Taydakov, M. L. Kuznetsov and V. Y. Kukushkin, *Inorg. Chem.*, 2022, **61**, 8670–8684.
26 L. Skorka, M. Filapek, L. Zur, J. G. Malecki, W. Pisarski, M. Olejnik, W. Danikiewicz and S. Krompiec, *J. Phys. Chem. C*, 2016, **120**, 7284–7294.
27 B. Balonova, T. H. Jones, A. E. True, S. M. Hetherington and B. A. Blight, *RSC Adv.*, 2024, **14**, 34288–34297.
28 K. Choroba, J. Palion-gazda, M. Penkala, P. Rawicka and B. Machura, *Dalton Trans.*, 2024, **2**, 17934–17947.
29 C. Jiang and T. S. Teets, *Inorg. Chem. Front.*, 2024, **11**, 1501–1510.
30 P. Gayen, U. Das and S. Banerjee, *J. Phys. Chem. A*, 2020, **124**, 4654–4665.
31 J. Li, P. I. Djurovich, B. D. Alleyne, M. Yousufuddin, N. N. Ho, J. C. Thomas, J. C. Peters, R. Bau and M. E. Thompson, *Inorg. Chem.*, 2005, **44**, 1713–1727.
32 Y. You and S. Y. Park, *J. Chem. Soc., Dalton Trans.*, 2009, **9226**, 1267–1282.
33 R. Mukherjee, *Coord. Chem. Rev.*, 2000, **203**, 151–218.
34 M. Viciano Chumillas, S. Tanase, L. J. de Jongh and J. Reedijk, *Eur. J. Inorg. Chem.*, 2010, **2010**, 3403–3418.
35 T. Hajra, J. K. Bera and V. Chandrasekhar, *Aust. J. Chem.*, 2011, **64**, 561–566.
36 M. A. Halcrow, *Dalton Trans.*, 2009, **9226**, 2059–2073.
37 V. Chandrasekhar, B. Mahanti, P. Bandipalli and K. Bhanuprakash, *Inorg. Chem.*, 2012, **51**, 10536–10547.
38 J. L. Liao, P. Rajakannu, P. Gnanasekaran, S. R. Tsai, C. H. Lin, S. H. Liu, C. H. Chang, G. H. Lee, P. T. Chou, Z. N. Chen and Y. Chi, *Adv. Opt. Mater.*, 2018, **6**, 1800083.
39 G. Comas-Vilà and P. Salvador, *Phys. Chem. Chem. Phys.*, 2025, **27**, 10482–10491.
40 C. Hansch, A. Leo and R. W. Taft, *Chem. Rev.*, 1991, **91**, 165–195.
41 K. Hasan, A. K. Bansal, I. D. W. Samuel, C. Roldán-Carmona, H. J. Bolink and E. Zysman-Colman, *Sci. Rep.*, 2015, **5**, 12325.
42 D. L. Davies, M. P. Lowe, K. S. Ryder, K. Singh and S. Singh, *Dalton Trans.*, 2011, **40**, 1028–1030.

43 X. Yang, X. Xu, J. Dang, G. Zhou, C.-L. Ho and W.-Y. Wong, *Inorg. Chem.*, 2016, **55**, 1720–1727.
44 X. Yang, X. Chen, J. Dang, Y. Sun, Z. Feng, Z. Tian, G. Zhou and Z. Wu, *Chem. Eng. J.*, 2020, **391**, 123505–123517.
45 E. Kabir, Y. Wu, S. Sittel, B.-L. Nguyen and T. S. Teets, *Inorg. Chem. Front.*, 2020, **7**, 1362–1373.
46 M. Nonoyama, *Bull. Chem. Soc. Jpn.*, 1974, **47**, 767–768.
47 G. Mezei and R. G. Raptis, *Inorg. Chim. Acta.*, 2004, **357**, 3279–3288.
48 (*a*) F. Scarpelli, A. Ionescu, L. Ricciardi, P. Plastina, I. Aiello, M. La Deda, A. Crispini, M. Ghedini and N. Godbert, *Dalton Trans.*, 2016, **45**, 17264–17273; (*b*) A. S. Inonkin, Y. Wang, W. J. Marshall and V. A. Petrov, *J. Organomet. Chem.*, 2007, **692**, 4809–4827.
49 D. A. Bardwell, L. Horsburgh, J. C. Jeffery, L. F. Joulic, M. D. Ward, I. Webster and L. J. Yellowlees, *J. Chem. Soc. Dalton Trans.*, 1996, **12**, 2527–2531.
50 H. Jude, F. N. Rein, P. S. White, D. M. Dattelbaum and R. C. Rocha, *Inorg. Chem.*, 2008, **47**, 7695–7702.
51 V. Chandrasekhar, T. Haira, J. K. Bera, S. M. W. Rahaman, N. Satumtira, O. Elbjeirami and M. A. Omary, *Inorg. Chem.*, 2012, **51**, 1319–1329.
52 X. Yuan, S. Zhang and Y. Ding, *Inorg. Chem. Commun.*, 2012, **17**, 26–29.
53 M. Y. Wong, G. Xie, C. Tourbillon, M. Sandroni, D. B. Cordes, A. M. Z. Slawin, I. D. W. Samuel and E. Zysman-Colman, *Dalton Trans.*, 2015, **44**, 8419–8432.
54 A. M'Hamedi, M. A. Fox, A. S. Batsanov, H. A. Al-Attar, A. P. Monkman and M. R. Bryce, *J. Mater. Chem. C*, 2017, **5**, 6777–6789.
55 G. Li, D. G. Congrave, D. Zhu, Z. Su, M. R. Bryce, G. Li, D. G. Congrave, D. Zhu, Z. Su and R. Bryce, *Polyhedron*, 2018, **140**, 146–157.
56 J. I. Goldsmith, W. R. Hudson, M. S. Lowry, T. H. Anderson and S. Bernhard, *J. Am. Chem. Soc.*, 2005, **127**, 7502–7510.
57 R. D. Costa, G. Fernández, L. Sánchez, N. Martín, E. Ortí and H. J. Bolink, *Chem.–Eur. J.*, 2010, **16**, 9855–9863.
58 A. Auffrant, A. Barbieri, F. Barigelletti, J. P. Collin, L. Flamigni, C. Sabatini and J. P. Sauvage, *Inorg. Chem.*, 2006, **45**, 10990–10997.
59 A. Auffrant, A. Barbieri, F. Barigelletti, J. Lacour, P. Mobian, J. P. Collin, J. P. Sauvage and B. Ventura, *Inorg. Chem.*, 2007, **46**, 6911–6919.
60 D. Di Censo, S. Fantacci, F. De Angelis, C. Klein, N. Evans, K. Kalyanasundaram, H. J. Bolink, M. Grätzel and M. K. Nazeeruddin, *Inorg. Chem.*, 2008, **47**, 980–989.
61 R. D. Costa, F. Monti, G. Accorsi, A. Barbieri, H. J. Bolink, E. Ortí and N. Armaroli, *Inorg. Chem.*, 2011, **50**, 7229–7238.
62 M. B. Robin and P. Day, *Adv. Inorg. Chem. Radiochem.*, 1968, **10**, 247–422.
63 A. Singh, P. Yadav, S. Singh, P. Kumar, S. Srikrishna and V. P. Singh, *J. Mater. Chem. C*, 2023, **11**, 13056–13066.
64 M. J. Frisch, G. W. Trucks, H. B. Schlegel, G. E. Scuseria, M. A. Robb Jr. J. R. Cheeseman, J. A. Montgomery, T. Vreven, K. N. Kudin, J. C. Burant, J. M. Millam, S. S. Iyengar, J. Tomasi, V. Barone, B. Mennucci, M. Cossi, G. Scalmani, N. Rega, G. A. Petersson, H. Nakatsuji, M. Hada, M. Ehara, K. Toyota, R. Fukuda, J. Hasegawa, M. Ishida, T. Nakajima, Y. Honda, O. Kitao, H. Nakai, M. Klene, X. Li, J. E. Knox, H. P. Hratchian, J. B. Cross, C. Adamo, J. Jaramillo, R. Gomperts, R. E. Stratmann, O. Yazyev, A. J. Austin, R. Cammi, C. Pomelli, J. W. Ochterski, P. Y. Ayala, K. Morokuma, G. A. Voth, P. Salvador, J. J. Dannenberg, V. G. Zakrzewski, S. Dapprich, A. D. Daniels, M. C. Strain, O. Farkas, D. K. Malick, A. D. Rabuck, K. Raghavachari, J. B. Foresman, J. V. Ortiz, Q. Cui, A. G. Baboul, S. Clifford, J. Cioslowski, B. B Stefanov, G. Liu, A. Liashenko, P. Piskorz, I. Komaromi, R. L. Martin, D. J. Fox, T. Keith, M. . A. Al-Laham, C. Y. Peng, A. Nanayakkara, M. Challacombe, P. M. W. Gill, B. Johnson, W. Chen, M. W. Wong, C. Gonzalez and J. A. Pople, *Gaussian 03*, Gaussian, Inc., Pittsburgh, PA, 2003.
65 C. Adamo and V. Barone, *J. Chem. Phys.*, 1999, **110**, 6158–6170.
66 J. P. Perdew, K. Burke and M. Ernzerhof, *Phys. Rev. Lett.*, 1997, **78**, 1396.
67 K. L. Schuchardt, B. T. Didier, T. Elsethagen, L. Sun, V. Gurumoorthi, J. Chase, J. Li and T. L. Windus, *J. Chem. Inf. Model.*, 2007, **47**, 1045–1052.
68 V. Kumar and H. Singh, *Int. J. Res. Anal. Rev.*, 2017, **4**, 89–95.
69 P. Nemykin and V. N. Basu, *VMOdes Program*, 2001.
70 M. Cossi, N. Rega, G. Scalmani and V. Barone, *J. Comput. Chem.*, 2003, **24**, 669–681.
71 O. V. Dolomanov, L. J. Bourhis, R. J. Gildea, J. A. K. Howard and H. Puschmann, *J. Appl. Crystallogr.*, 2009, **42**, 339–341.
72 G. M. Sheldricka, *Acta Crystallogr., Sect. A*, 2015, **71**, 3–8.
73 CCDC 2415220: Experimental Crystal Structure Determination, 2026, DOI: 10.5517/ccdc.csd.cc2m27b9.